HAL
open science

Combined Structural Analysis and Molecular Dynamics Reveal Penicillin-Binding Protein Inhibition Mode with β-Lactones

Parker Flanders, Carlos Contreras-Martel, Nathaniel Brown, Joshua Shirley, Alexandre Martins, Kelsie Nauta, Andréa Dessen, Erin Carlson, Elizabeth Ambrose

To cite this version:

Parker Flanders, Carlos Contreras-Martel, Nathaniel Brown, Joshua Shirley, Alexandre Martins, et al.. Combined Structural Analysis and Molecular Dynamics Reveal Penicillin-Binding Protein Inhibition Mode with β-Lactones. ACS Chemical Biology, 2022, 17 (11), pp.3110-3120. 10.1021/acschembio.2c00503 . hal-03969300

HAL Id: hal-03969300

https://hal.science/hal-03969300v1

Submitted on 13 Oct 2023

HAL is a multi-disciplinary open access archive for the deposit and dissemination of scientific research documents, whether they are published or not. The documents may come from teaching and research institutions in France or abroad, or from public or private research centers.

L'archive ouverte pluridisciplinaire **HAL**, est destinée au dépôt et à la diffusion de documents scientifiques de niveau recherche, publiés ou non, émanant des établissements d'enseignement et de recherche français ou étrangers, des laboratoires publics ou privés.

ACS chemical biology

pubs.acs.org/acschemicalbiology

Articles

Combined Structural Analysis and Molecular Dynamics Reveal Penicillin-Binding Protein Inhibition Mode with β-Lactones

Parker L. Flanders, Carlos Contreras-Martel, Nathaniel W. Brown,[%] Joshua D. Shirley,[%] Alexandre Martins, Kelsie N. Nauta, Andréa Dessen, Erin E. Carlson,* and Elizabeth A. Ambrose*

Cite This: https://doi.org/10.1021/acschembio.2c00503

Read Online

ACCESS | Metrics & More | Article Recommendations | Supporting Information

ABSTRACT: β-Lactam antibiotics comprise one of the most widely used therapeutic classes to combat bacterial infections. This general scaffold has long been known to inhibit bacterial cell wall biosynthesis by inactivating penicillin-binding proteins (PBPs); however, bacterial resistance to β-lactams is now widespread, and new strategies are urgently needed to target PBPs and other proteins involved in bacterial cell wall formation. A key requirement in the identification of strategies to overcome resistance is a deeper understanding of the roles of the PBPs and their associated proteins during cell growth and division, such as can be obtained with the use of selective chemical probes. Probe development has typically depended upon known PBP inhibitors, which have historically been thought to require a negatively charged moiety that mimics the C-terminus of the PBP natural peptidoglycan substrate, D-Ala-D-Ala. However, we have identified a new class of β-lactone-containing molecules that interact with PBPs, often in an isoform-specific manner, and do not incorporate this C-terminal mimetic. Here, we report a series of structural biology experiments and molecular dynamics simulations that we utilized to evaluate specific binding modes of this novel PBP inhibitor class. In this work, we obtained <2 Å resolution X-ray structures of four β-lactone probes bound to PBP1b from *Streptococcus pneumoniae*. Despite their diverging recognition modes beyond the site of covalent modification, these four probes all efficiently labeled PBP1b, as well as other PBPs from *S. pneumoniae*. From these structures, we analyzed protein−ligand interactions and characterized the β-lactone-bound active sites using *in silico* mutagenesis and molecular dynamics. Our approach has clarified the dynamic interaction profile in this series of ligands, expanding the understanding of PBP inhibitor binding.

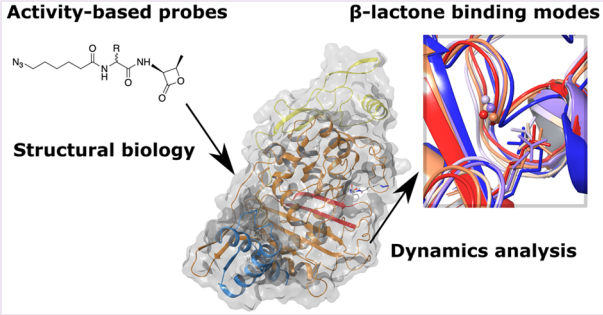

Downloaded via INIST-CNRS on October 1, 2022 at 10:40:07 (UTC).
See https://pubs.acs.org/sharingguidelines for options on how to legitimately share published articles.

■ INTRODUCTION

Penicillin-binding proteins (PBPs) are the primary targets of β-lactam antibiotics and constitute an essential class of enzymes that are ubiquitously expressed in eubacteria. These proteins play critical roles in the biosynthesis of peptidoglycan (PG), the main component of the bacterial cell wall, a polymeric matrix that provides structural rigidity to the cell wall and enables protection from osmotic pressure.[1] PBP inhibition or deregulation can lead to defects in cell shape and weakening of the PG, and may eventually lead to cell lysis and death. Several PBPs are also involved in the development of resistance to β-lactam antibiotics.[2−7]

PBPs are key members of both the divisome and the elongasome, large protein complexes that are required for division and cell elongation, respectively. While the PBPs have been reported to interact with several members of both complexes,[7−10] significant gaps remain in our understanding of how the PBPs facilitate bacterial cell growth, wall elongation, and division. Depending on the species, bacteria are known to encode 4−18 PBPs that fall into three categories. Bifunctional class A PBPs (aPBPs) possess glycosyltransferase and transpeptidase (TP) domains that cross-link glycan strands and stem peptides, respectively.[11] Monofunctional class B PBPs (bPBPs) possess only TP domains, and work in tandem with glycosyltransferases of the SEDS (shape, elongation, division, sporulation) protein family to synthesize PG.[12,13] Finally, monofunctional class C PBPs (cPBPs) are D,D-carboxypeptidases (CPs) that possess a TP domain and cleave the terminal D-Ala residue of the stem-peptide chain, thus regulating PG cross-linking.[14]

While PBPs are critical drug targets for the treatment of bacterial infections, the roles of these proteins in bacterial growth and division have also been the subjects of intense investigation.[7,8] Our work has chiefly focused on the PBPs found in *Streptococcus pneumoniae*, the primary causative agent

Received: June 14, 2022
Accepted: September 15, 2022

© XXXX American Chemical Society

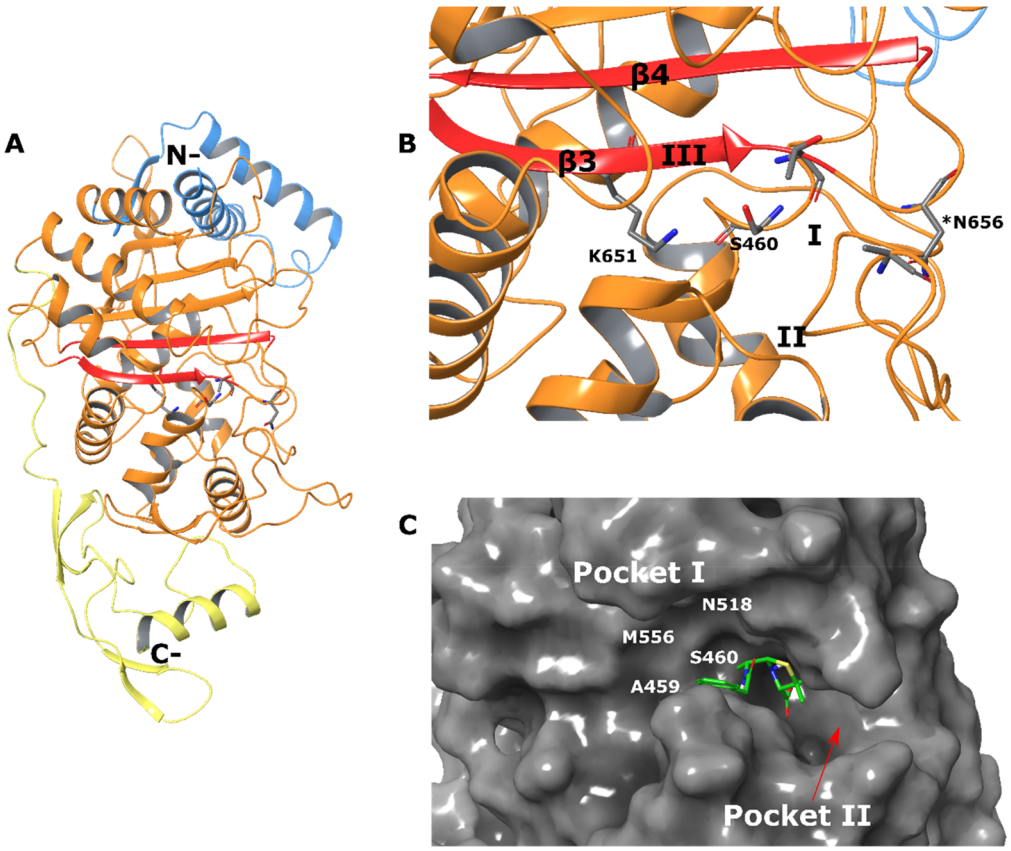

Figure 1. Overview of the apoPBP1b structure in *Streptococcus pneumoniae* (PBP ID 7ZUH). (A) The GT/TP interdomain "head" region (blue) is the N-terminal of the catalytic TP "body" region (orange) along with β3 and β4 labeled in red and is followed by the C-terminal region (yellow). (B) Active-site view of apo PBP1b. The catalytic serine is shown in motif I (SXXK) with motif II (S(Y)XN(C)) highlighted directly below and motif III (K(H)T(S)G) highlighted on β3. The asterisk marks the active-site mutation of N656G on the β3−β4 loop. (C) Surface view of the PBP1b active site complexed with a boronic acid inhibitor (PDB: 2Y2K). Pocket I is illustrated, with pocket II indicated by an arrow behind the surface view.

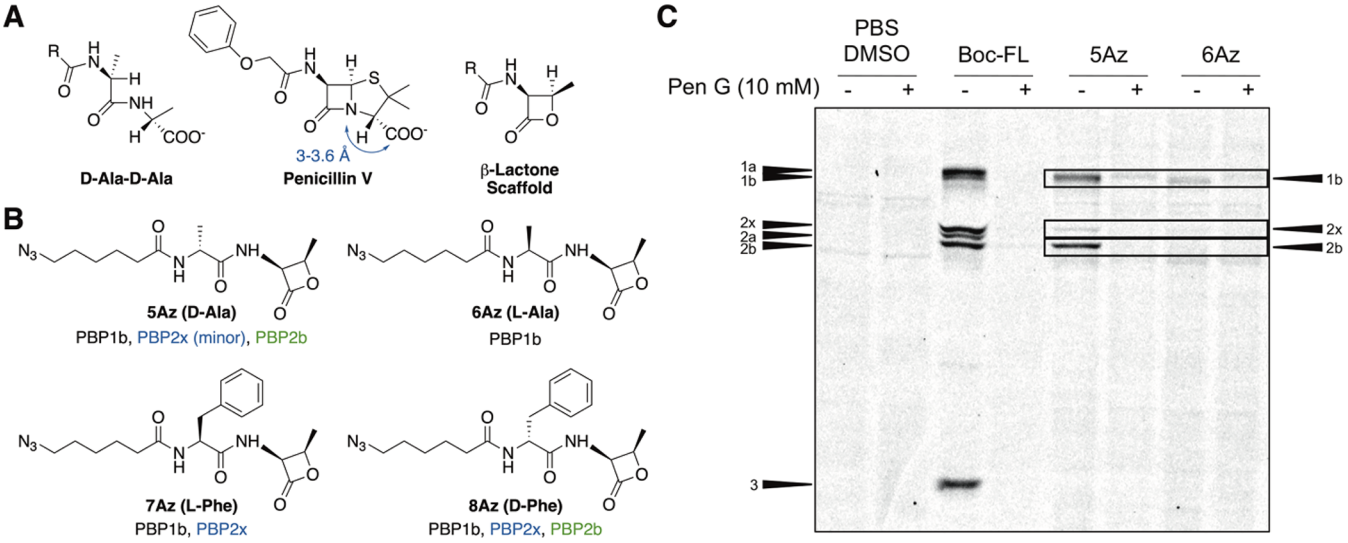

Figure 2. Bioorthogonal β-lactone-based probes were designed to enable the detailed study of PBP−lactone interactions. (A) The natural substrate of the PBPs bears a D-Ala-D-Ala group that is mimicked by β-lactam drugs, such as penicillin V. All clinically utilized β-lactams possess a negatively charged group near the electrophilic carbonyl (highlighted in blue). While the lactone scaffold mimics the stereochemical orientation of these two molecules, it lacks a negatively charged group. (B) Probe library to explore the PBP labeling in live *S. pneumoniae*. Colors emphasize PBP binding similarities between the probes. (C) Gel-based analysis shows PBP selectivity of probes **5Az** and **6Az**, as well as their competition with penicillin G (10 mM). Boc-FL (fluorophore conjugated to Pen V, depicted in part A) labels all PBPs in *S. pneumoniae*, while the lactone-based probes are more selective. Boc-FL (5 μM) or 100 μM **5Az** or **6Az** with 50 μM fluorescein-alkyne.

https://doi.org/10.1021/acschembio.2c00503
ACS Chem. Biol. XXXX, XXX, XXX−XXX

of community-acquired pneumonia, otitis media, and bacterial meningitis—diseases that have a significant global burden.[15] *S. pneumoniae* expresses six PBPs: three class A (PBP1a, 1b, 2a), two class B (PBP2x, PBP2b), and one type-5 class C (PBP3).[16] The effectiveness of β-lactam antibiotics against *S. pneumoniae* infections has been challenged by increasing resistance to these drugs, which underscores the need for new scaffolds that target these enzymes.[17] *S. pneumoniae* is also an ideal model organism in which to perform PBP functional analyses and to explore the utility of potential new chemical probes and inhibitors, as it possesses a relatively small collection of PBPs and utilizes both division and elongation machineries during its growth and division processes.[18]

PBPs possess three regions, in which the "head" and "neck" areas correspond approximately to the N-terminal and linker domains and the "body" region incorporates the C-terminal TP domain (Figure 1a). The TP domain comprises a central β-sheet surrounded by α-helices and is highly conserved in multiple PBP structures (TPs and CPs). The PBP active site features three highly conserved motifs located within the TP domain, to which β-lactams bind. Motif I includes a SXXK sequence, where the conserved serine acts as the active-site nucleophile that either promotes the transformation of the native substrate (the C-terminal D-Ala-D-Ala moiety of the PG stem peptide) or covalently interacts with β-lactam drugs. Motif II possesses an S(Y)XN(C) sequence, and motif III includes K(H)T(S)G (Figure 1b). Despite the low sequence similarities among different PBPs, the overall structural conservation of these motifs is very high: the position of the conserved active-site residues often varies by less than 1 Å.[4,9,16,19−24] It is also of interest that the PBP active site can be described as an elongated tunnel, where inhibitor side chains are positioned in two distinct pockets. Pocket 1 is flat and located toward the back of the active site, pointing away from the β3−β4 flexible loop region. Pocket 2 is close to this loop region and harbors residues that stabilize aromatic rings in different inhibitors.[25]

Despite this structural and functional homology, the expression, spatiotemporal localization, and mechanisms of the individual PBPs are not fully understood. While the different functions of several PBPs have long been studied using methods such as deletion strains or fusion constructs (e.g., fluorescent or affinity tags), those strategies provide an incomplete picture, as they cannot specifically report on PBP catalytic activities. To overcome this limitation, we[26−28] and others[29,30] have utilized activity-based probes (ABPs) to selectively characterize PBPs in an activity-dependent manner. In general, these ABPs have relied upon modification of commercially available β-lactam scaffolds, which mimic the native stem peptide substrate of the PBPs (Figure 2a). However, our previous work has shown that the utility of these molecules is limited, as they often simultaneously inhibit numerous PBPs and/or target some PBPs only rarely, making the development of tools to explore these isoforms difficult (e.g., PBP2a and PBP2b in *S. pneumoniae*).[27,28] Thus, expansion of the chemical space used for the design of PBP-targeted probe molecules is essential and may also lead to the identification of new scaffolds for therapeutic development. We have reported that β-lactones, based on a 3-amino-4-methyl-2-oxetanone scaffold, can specifically target the PBPs in a full proteome.[25,31] This result was not anticipated, as this scaffold lacks a negatively charged moiety to mimic the carboxy terminus of the native substrate (within 3−3.6 Å of carbonyl carbon) that is thought to be essential for active-site recognition and is found in all clinically approved PBP inhibitors (highlighted in blue, Figure 2a).[32] This striking result, together with the fact that alteration of a single stereocenter in several of the β-lactone analogues drastically changes their PBP-isoform selectivity, prompted us to further explore the binding mode(s) of this novel PBP inhibitor class.

Here, we present high-resolution structures of four β-lactone probes in complex with PBP1b*, a soluble form of *S. pneumoniae* PBP1b. Our structural data show that these molecules bind to the PBP active site in the absence of a negatively charged functionality and also point to significant variations in ligand−receptor interactions resulting from relatively minor changes in probe structure. Next, these novel structures were subjected to molecular modeling and dynamics simulations to further elucidate the protein−ligand interaction profile across this series of probes, as well as pinpoint key structural features of the PBP1b active site in ligand-bound and ligand-free states. Our results reveal key binding modes of non-anionic β-lactone ligands to the PBP active site and provide a necessary foundation to guide the structure-based design of novel PBP ligand classes in future work.

■ RESULTS

Probe Selection and Characterization. We previously reported that β-lactone-containing molecules selectively target the PBPs in live *S. pneumoniae*, providing a new scaffold for probing this class of enzymes.[31,33] Importantly, β-lactones were found to target several PBPs that are not effectively inhibited by traditional β-lactam molecules. Using a gel-based assay in which *S. pneumoniae* were treated with each probe followed by a copper-catalyzed azide−alkyne cycloaddition (CuAAC) reaction with an alkyne-functionalized fluorescein to act as the reporter group, we determined that β-lactone-based probes functionalized with a phenylalanine moiety, **7Az** (L-Phe) and **8Az** (D-Phe), labeled pneumococcal PBP1b and PBP2x, or PBP1b, PBP2x, and PBP2b, respectively (Figure 2b).[31,33] We were excited to note that one of the stereoisomers labeled PBP2b (**8Az**, D-Phe-derived molecule), which is difficult to target with β-lactams.[28,34] Given this significant difference in the binding profiles of probes **7Az** and **8Az**, we sought to evaluate their PBP-binding interactions at the molecular level through a combination of protein crystallography and molecular modeling.

To expand our studies, we also included β-lactone-based probes bearing an alanine group to mimic the C-terminus of the natural substrate stem peptide [**5Az** (D-Ala), **6Az** (L-Ala)] (Figure 2b and c). We previously reported that, when directly appended to a fluorophore, Ala-functionalized scaffolds (**5** and **6**) labeled similar PBPs to Phe-bearing structures (**7** and **8**).[31] However, we also found that the identity of the appended fluorophore can drastically affect PBP labeling. This suggested that a comparison study should instead be performed with a suite of probes that only bear the much smaller azide.[31,33] Indeed, we recently reported major differences in the labeling profiles of clickable Phe-bearing structures (**7** and **8**) in comparison to fluorophore-functionalized molecules,[33] and herein, we found that the PBP labeling profiles of **5Az** and **6Az** were substantially different from the fluorophore-conjugated derivatives (Figure 2b and c; Supporting Information Figures 1 and 2). Probe **5Az** (D-Ala) labels PBP1b and PBP2b in a dose-dependent manner (minor PBP2x labeling at high concen-

https://doi.org/10.1021/acschembio.2c00503
ACS Chem. Biol. XXXX, XXX, XXX−XXX

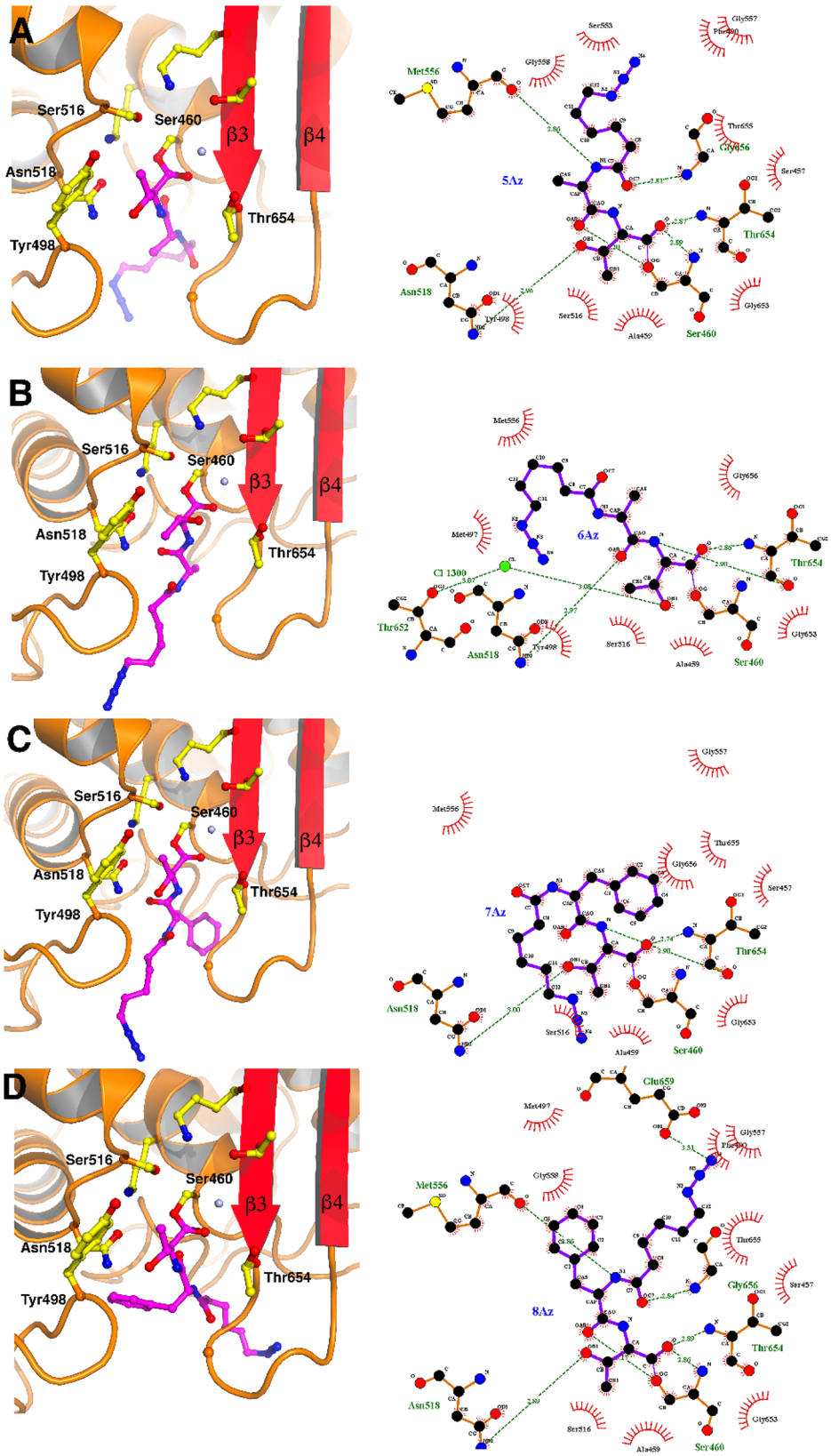

Figure 3. PBP1b* active-site crystal structures obtained for complex **5Az** (A, PDB 7ZUI), **6Az** (B, PDB 7ZUJ), **7Az** (C, PDB 7ZUK), and **8Az** (D, PDB 7ZUL). (left panels) Side chains are shown as ball-and-stick, with ligand carbon atoms in purple and protein carbon atoms in yellow. (right panels) Ligplot[35] analyses of the protein−ligand interactions for the probes within the cleft.

tration; Figure 2c and Supporting Information Figure 2), while fluorophore-conjugated derivatives of **5** labeled as few as two PBPs or up to five PBPs, depending on the fluorophore.[31] We also found that **6Az** (L-Ala) labeled only PBP1b (Figure 2c and Supporting Information Figure 2), while the fluorophore-functionalized analogues labeled PBP1b and/or PBP2x. These

https://doi.org/10.1021/acschembio.2c00503
ACS Chem. Biol. XXXX, XXX, XXX−XXX

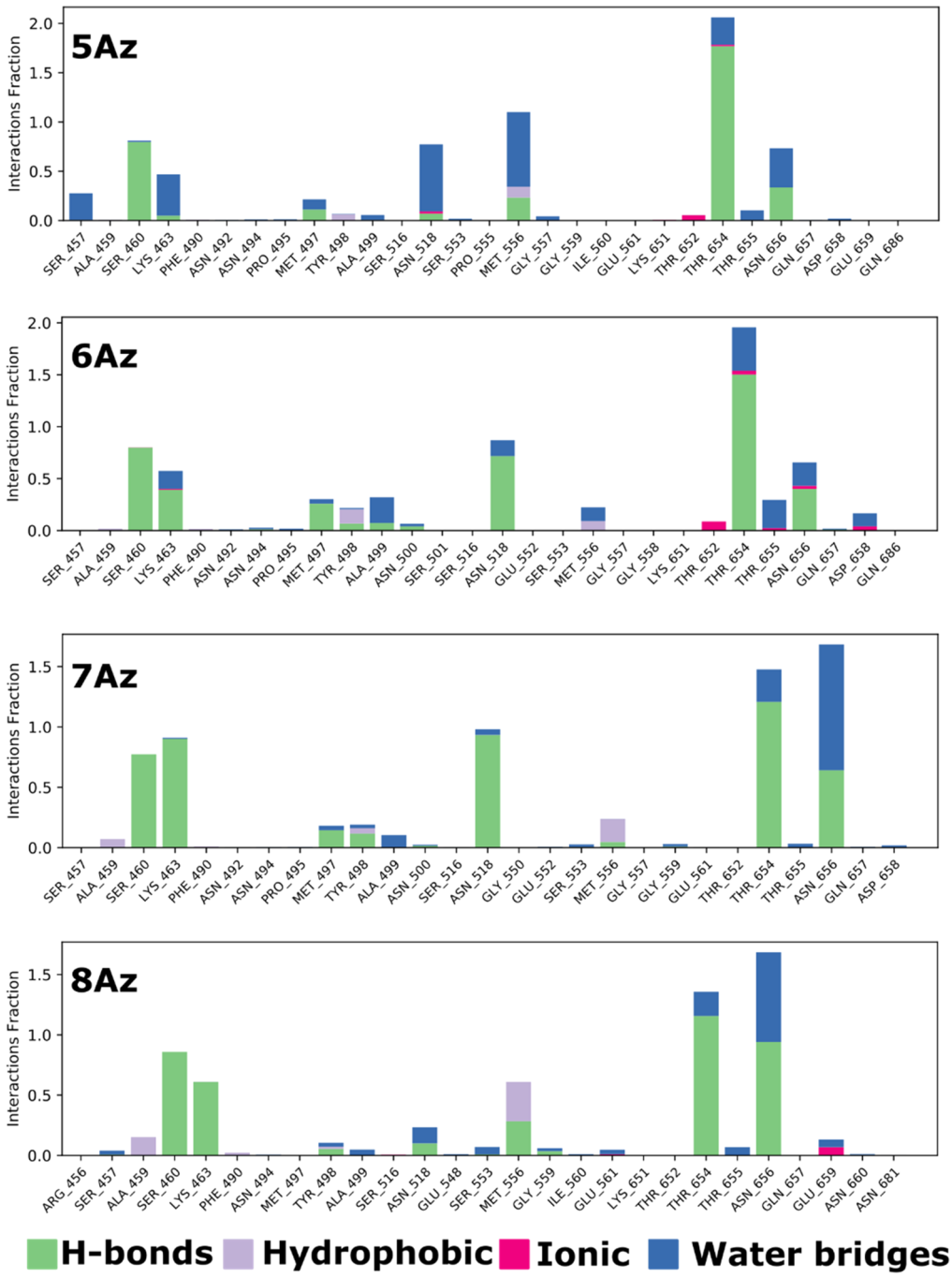

Figure 4. Stacked bar plot highlighting ligand IFs for **5Az**, **6Az**, **7Az**, and **8Az** per residue throughout the MD simulation, where values over 1.0 indicate multiple interactions are made. Interaction types are labeled by color.

data provide further evidence that fluorophores can drastically change the ability of probes to interact with several PBPs, often in unpredictable ways that are unlikely to be related to discrete binding interactions in the active site (e.g., hydrophobic interactions on the protein surface).

With this collection of simplified probes in hand, we could now evaluate PBP binding to further understand how steric bulk and spatial orientation of the molecules can affect interactions within the PBP active site, and provide clues about why a negatively charged moiety is not required for binding. Given that all four probes (**5Az**−**8Az**) labeled wild-type PBP1b in *S. pneumoniae* cells, we used this protein as a model to provide the first structural information about β-lactone−PBP binding and to directly compare their binding interactions. Indeed, while all of the compounds labeled PBP1b, the change from L-Ala to D-Ala resulted in PBP2b labeling. Interestingly, the D-Phe-containing probe also labeled PBP2b, while the L-Phe molecule did not, perhaps indicating that a D-configuration at this position may contribute to PBP2b binding. Finally, both Phe-containing probes labeled PBP2x while the Ala-decorated molecules did not, which could indicate a larger binding pocket to accommodate this bulk. Consistent with this, PBP2x was one of the most commonly inhibited pneumococcal PBPs with a collection of 42 β-lactams, further suggesting that the active site can accommodate a variety of molecular architectures.[27,34]

https://doi.org/10.1021/acschembio.2c00503
ACS Chem. Biol. XXXX, XXX, XXX−XXX

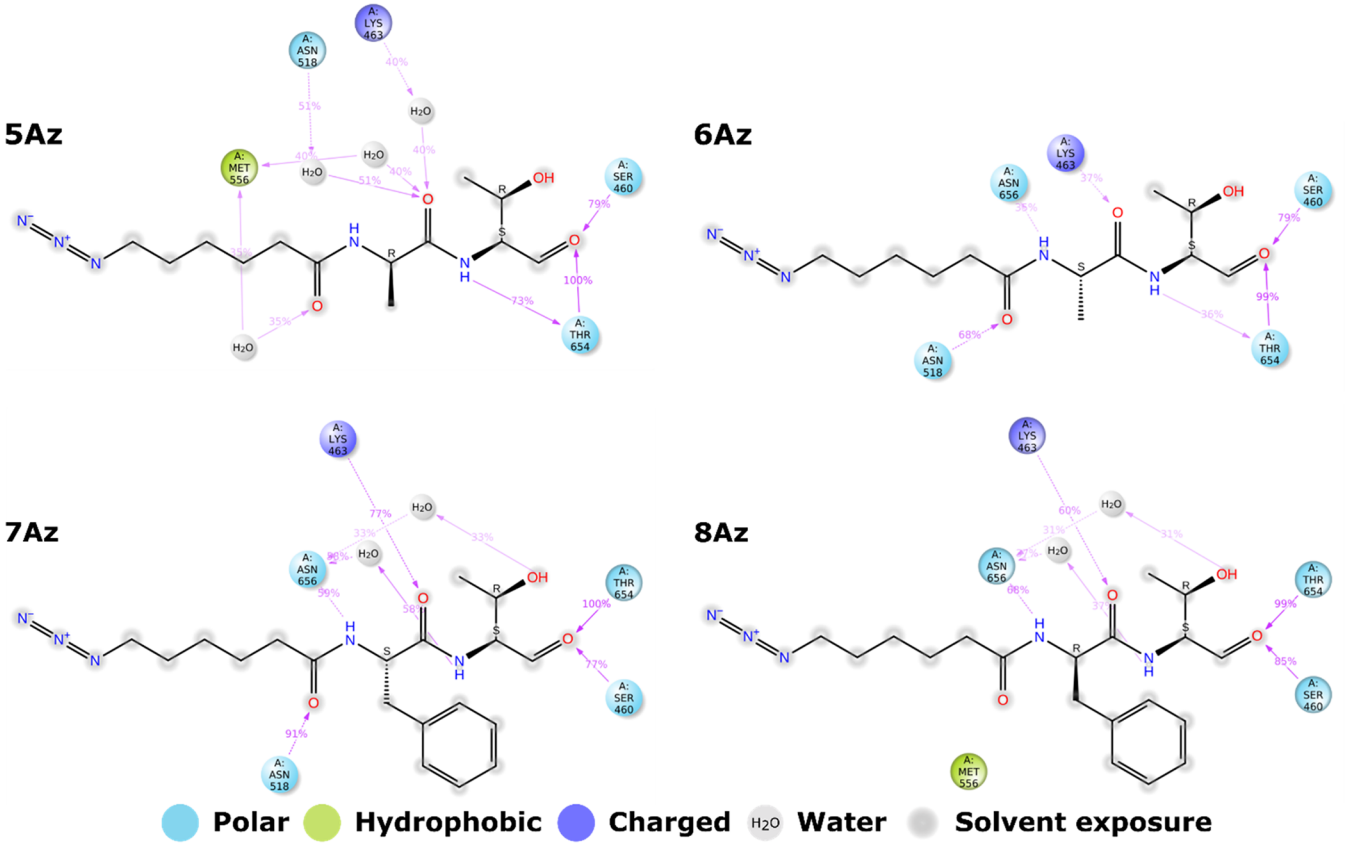

Figure 5. Protein–ligand interaction diagrams for **5Az**, **6Az**, **7Az**, and **8Az** from 30 ns MD simulations. The ligand interaction plots display both hydrogen bonding and water bridges, where the interaction % indicates the percentage of the simulation in which that interaction is occurring. The intensity of the purple interaction arrow corresponds to the interaction %.

Crystal Structures of PBP1b* Complexes. To obtain high-resolution structural data, we crystallized a soluble form of *S. pneumoniae* PBP1b, that harbors an Asn656Gly mutation at the β3–β4 loop to maintain an open active site (PBP1b*).[32] All four probes were soaked into PBP1b* crystals, and data were collected at the ESRF synchrotron in Grenoble, France, allowing us to obtain structures of **5Az**, **6Az**, **7Az**, and **8Az** covalently bound in the active site of PBP1b* (PDB IDs 7ZUI, 7ZUJ, 7ZUK, and 7ZUL, respectively). In all four structures, most ligand atoms were easily visualized and traced in the electron density maps, except for the often highly flexible azide tails.

The three conserved catalytic motifs in the PBP1b* active site are Ser460-Thr461-Thr462-X-Lys463, which incorporates the nucleophilic Ser460, Ser516-X-Asn518, and Lys651-Thr652-Gly653. In all four complex crystal structures, electron density corresponding to the probes indicates that, as expected, Oγ of Ser460 is covalently associated with the ligands. In addition to this covalent bond, several ligand–receptor interactions are common to all four structures, including hydrogen bonding between Asn518 and the secondary alcohol or the first amide carbonyl on the probe. We also observed interactions with the backbones of Thr654 and Ser460. These two residues form part of a conserved pocket known as the "oxyanion hole" that stabilizes the Michaelis complex prior to acylation; its formation is a key and obligatory step in ligand binding.[36] In all β-lactone structures, a Cl^- atom (indicated as a gray sphere in Figure 3) is located in close proximity (3.8 Å) to Thr652 and Lys651 on motif III. Ligplots[35] indicate that the primary interaction with the Cl^- atom is via Thr652, although Lys651 points toward the ion as well. The binding modes of **5Az**, **6Az**, **7Az**, and **8Az** within the PBP1b* active site are broadly similar to that in which previously published boronic acid inhibitors (Figure 1) bind to pocket I of PBP1b*, where the hydrophobic regions are located proximally to the β3/β4 loop and the highly flexible azide moieties point to the exterior of the active site.[25] Notably, the phenyl group of **8Az** is also stabilized by a groove formed by the side chains of Met556, Ile519, and Phe490 (Figure 3d).

Molecular Dynamics Simulations of PBP1b* X-ray Structures. Next, we utilized molecular dynamics (MD) to probe PBP1b* active-site conformational flexibility, capturing a wider variety of dynamic intermolecular interactions between both β-lactones and PBP1b and identifying short- and long-time-scale ligand–receptor interactions that may affect inhibitor potency. In this study, we utilized *in silico* mutagenesis to regenerate the wild-type PBP1b active site and MD simulations to capture dynamic intermolecular interactions between these compounds and PBP1b. MD was used not only to corroborate experimentally observed interactions but also to rule out interactions that, while observed in crystallographic structures, may not maintain themselves over a significant time scale. Furthermore, our approach allowed for the characterization of a flexible protein active site when bound to a flexible ligand, including the study of solvent dynamics. To establish the simulation time necessary for extensive conformational sampling, we first calculated Cα root-mean-square deviation (RMSD) values, together with the cosine content of the principal components (PCs),[37] for PBP1b in preliminary dynamics runs. We found that a 30 ns

https://doi.org/10.1021/acschembio.2c00503
ACS Chem. Biol. XXXX, XXX, XXX–XXX

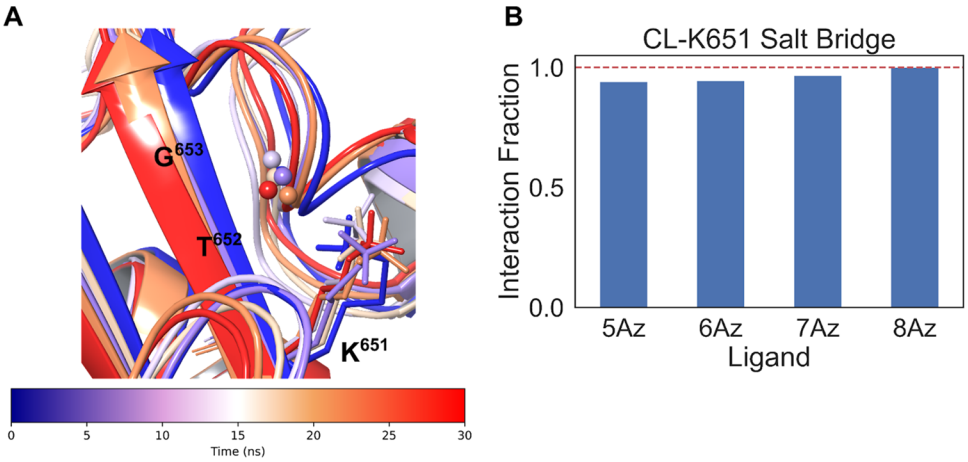

Figure 6. (A) Trajectory snapshots of the protein-bound chloride ion in **7Az**−PBP1b, taken every 6 ns, emphasizing its proximity to the conserved KTG motif, as well as persistent salt bridges in all structures. (B) Bar plot of chloride ion and the Lys651 salt bridge interaction fractions in each protein−ligand complex. The red dashed line indicates a 100% interaction fraction.

simulation time enabled sufficient system sampling, with protein RMSD values stabilizing between 1 and 2 Å, and the cosine content of the PCs consistently less than 0.7 (Supporting Information Figure 4); all subsequent dynamics simulations were therefore carried out for 30 ns.

Molecular dynamics enabled us to prioritize the PBP1b ligand−receptor interactions that most strongly contribute to ligand binding, as assessed by calculated interaction fraction (IF). IF is defined as the simulation time in which an intermolecular interaction occurs divided by the total dynamics runtime, as indicated by intermolecular distance and angle criteria for that interaction type. For example, an IF of 0.5 indicates that an interaction takes place during 50% of the entire simulation, and a fraction greater than 1 indicates multiple persistent ligand−receptor interactions. In all of our protein−ligand dynamics simulations, the carbonyl oxygen in the acyl−serine bond maintained interaction with the backbone of both Ser460 and Thr654, as indicated by IF > 1 for Thr654 in all ligands (Figure 4). From our X-ray structures, we observed both **6Az** and **7Az** (L-configuration) interact with Asn518 (motif II) via a direct hydrogen bond with the amide carbonyl (Figure 5). However, dynamics predicted that the Asn518−**7Az** interaction is far more persistent than that of Asn518−**6Az**, with IF values of 91% and 68%, respectively, which is likely due to the presence in **7Az** of a phenyl ring that securely occupies pocket I of the receptor. Compound **5Az** maintains a water bridge with Asn518 for 51% of the 30 ns simulation, along with multiple water bridges to Met556. In contrast, **8Az** (D-configuration) does not significantly engage with motif II. The orientation of **8Az** allows for linker amide interactions with both Asn656 and Met556 but not with Asn518 due to the D-Phe group in **8Az** occupying the space between Asn518 and β3. Notably, the modeled Asn656 residue engaged in H-bonding with all β-lactone probes. The ubiquitously observed chloride ion (Figure 3) was predicted to maintain interaction with the ligand via Thr652 from initial structures. Despite this, its IF of <10% suggests that interactions involving this Cl^- are not significant. Furthermore, the X-ray structures indicated an interaction between the azide tail of **8Az** and Glu659. This interaction fraction is <10% and is also predicted as not significant.

In all ligand-bound simulations, we confirmed the persistence of the experimentally observed chloride ion (Figure 3) occupying a pocket proximal to motif III (KTG) on β3. This chloride ion is being stabilized by a salt bridge with the protonated Lys651 (Figure 6a). Study of motif III has demonstrated it to be vital for catalysis in other PBPs, serving as an electrostatic anchor for the terminal carboxylate of the D-Ala natural substrate, or the carboxylate of β-lactams (*vide supra*).[38,39] We hypothesize that the absence of a carboxylate in the β-lactone ligands allows for an anion binding site to form in this pocket, as Lys651 and Thr652 participate in a dense hydrogen bond network with a water molecule and the catalytic serine in a previously solved apo-PBP1b* structure (PDB: 2BG1[16]). In other solved PBP1b* structures with carboxylate-containing small molecules, this carboxylate interacts directly with motif III via hydrogen bonding with Thr652.[16] From previous data as well as our own, we hypothesize that this pocket becomes available for anion binding upon active-site rearrangement following ligand binding, enabling the lactone-based probes to effectively bind the PBPs despite the lack of a negatively charged moiety. Figure 6b highlights the salt bridge interaction fraction between Lys651, located on motif III, and the observed chloride ion occupying the active-site pocket. In all ligand-bound structures, the IF for this salt bridge was greater than 90%, providing a rationale for the high occupancy of the Cl^- ion across structures.

Analysis of ligand root-mean-square fluctuation (RMSF) with respect to the protein backbone can be used to compare the stability of ligands within the same active site. In addition, ligand RMSF with respect to the initial ligand pose can be used to compare the movement of the ligand to its initial experimentally determined binding mode. We observed lower RMSF values with respect to both protein and ligand for **5Az** when compared to **6Az**. This is likely due to the additional stabilizing water bridges present with **5Az**. RMSF values with respect to protein and ligand were similar for **7Az** and **8Az**. However, **7Az** exhibited a higher RMSF in its phenyl side chain and bioorthogonal handle. The phenyl ring of **8Az** was observed in both X-ray crystallography and molecular dynamics results to be stabilized by Met556 (Supporting Information Figures 5 and 6) with RMSF values for the covalently bound region remaining relatively low (<2 Å) across the probes. As expected, the bioorthogonal handle and flexible linker region of the ligands exhibited the highest RMSF values,

https://doi.org/10.1021/acschembio.2c00503
ACS Chem. Biol. XXXX, XXX, XXX−XXX

as they are the most dynamic portion of the molecules. Overall, our MD simulations reliably reproduced many of the protein−ligand interactions observed via X-ray crystallography, indicating the suitability of these calculations for the PBP1b−ligand systems studied here, and were also able to capture key interactions with Asn656. The MD calculations also successfully probed solvent dynamics within the PBP1b active site, including stable ligand water bridges.

DISCUSSION

β-Lactones represent a novel class of PBP inhibitors and a valuable tool for the study of PBPs in an activity-dependent manner—something that is not possible with traditional biochemical methods that have been applied to PBPs. Labeling experiments with these ABPs have revealed unique selectivity profiles among **5**/**6**/**7**/**8Az** despite their chemical similarity, illustrating key features that can be exploited to optimize ligand binding. For example, PBP1b appears to be fairly promiscuous in the lactones that it will bind. In addition, PBP2x may require a relatively large and/or hydrophobic group for binding, as it was only labeled with Phe-containing probes and not with the Ala-functionalized derivatives. Finally, PBP2b appears to favor probes with a D-configuration in the diversity element, as it was only inhibited by **5Az** and **8Az**.

Previous structural analyses of the PBP1b* transpeptidase domain revealed distinct conformations for the *β*3/*β*4 loop that lies at the entrance of the active site.[16] Our structural biology and dynamics results confirm the acylation by these *β*-lactone probes within the PBP1b active site and call attention to the conservation of participating active-site residues in the natural peptide substrate, *β*-lactams, and now *β*-lactones. It has been noted previously that in *β*-lactams, along with the natural D-Ala peptide substrate, there are three conserved binding features.[36] First, the substrate's amide group sits between Asn from the second conserved motif and the *β*3 loop (Asn518 in PBP1b). Second, the terminal peptide carboxylate or the *β*-lactam carboxylate interacts via hydrogen bonding with the KTG motif. Third, the carbonyl oxygen sits within the oxyanion hole. Here, our results further highlight these conserved binding events, now seen with *β*-lactones. While X-ray crystallography captured many of the direct interactions made with the more stable portion of the probe, molecular dynamics was needed to capture the interactions between flexible portions of the ligand with both the protein and solvent molecules. In lieu of a carboxylate group in the lactone-based probes, motif III appears to participate in the formation of an anion binding site. It has previously been noted that the conserved lysine of motif III in other PBPs serves as an "electrostatic anchor" to facilitate pre-covalent binding in carboxylate-containing ligands.[30] Strikingly, our data indicate that not all PBP inhibitors require this interaction for binding.

Our analyses via X-ray crystallography and molecular dynamics characterized the binding mode of *β*-lactones, as well as the active site of PBP1b in the presence of covalently bound *β*-lactones. We demonstrated conservation in protein−ligand interactions between this series of probes, as well as chemically distinct ligands observed previously. These results shed light on the "canonical" binding profiles between *β*-lactams, the D-Ala substrate, and now *β*-lactones. In characterizing the protein−ligand interactions and active site of a flexible system like PBP1b, a static perspective is insufficient to fully capture the relevant intermolecular interactions. In particular, we quantified the persistence of many solvent interactions and ligand interactions with Asn656 and identified empirically observed interactions that did not maintain for a significant time scale. Molecular dynamics simulations from crystallographic structures serve as a guide for the structural basis of *β*-lactone binding within PBP1b, as well as the optimization of these probes in future studies. Additionally, insight into these key interactions within a novel PBP binding chemotype provides foundational knowledge for the structure-based design and development of PBP inhibitors and probes in the future.

MATERIALS AND METHODS

Details of probe synthesis and gel-based characterization are found in the Supporting Information.

Molecular Modeling. Simulations in this study were performed with Maestro v.2021-3 (Schrodinger, Inc., New York). Complexes of PBP1b* crystallized with **5Az**, **6Az**, **7Az**, and **8Az** were first mutated from G656 to N656, with the lowest energy rotamer chosen. The azide handles present in all ligands were manually edited using the "3D Builder" to assign correct bond types and charges, followed by minimization of the modified atoms. Solvent atoms were kept in place. All structures were then prepared via the "Protein Preparation Tool" using default settings with termini capped.[40] Hydrogens were minimized via the OPLS4 force field.

Molecular Dynamics. Molecular dynamics simulations were performed using the Desmond software within Maestro (D.E. Shaw Research, New York).[41] The protein−ligand complexes were solvated in an orthogonal box of PCM water with a 10 Å buffer. The complexes were neutralized with Na^+ counterions in addition to 0.15 M NaCl. The solvated complexes were then relaxed and equilibrated using the default Desmond relaxation protocol. First, an NVT simulation with Brownian dynamics was performed at 10 K with small time steps and solute heavy atom restraints. A 12 ps NVT simulation was then performed at 10 K with solute heavy atom restraints. Next, a 12 ps NPT simulation at 10 K and 1 atm with solute heavy atom restraints was performed, followed by a 12 ps NPT simulation at 300 K and 1 atm with solute heavy atom restraints. Finally, a 24 ps NPT simulation at 300 K and 1 atm was performed with no atom restraints. Following this protocol, a 30 ns NPT simulation at 300 K and 1 atm was carried out with a 300 ps recording interval. Simulations were analyzed via the "Simulation Interaction Diagram" tool and trajectory analysis tools provided in the Maestro workspace. RMSD and RMSF figures were generated with Python 3.8.12 using matplotlib and seaborn libraries. The cosine content of the trajectory PCs was calculated with Python 3.8.12 using MDAnalysis and matplotlib libraries.[42]

PBP1b* Purification and Crystallization. PBP1b* was purified mostly as previously described.[32] PBP1b* crystals were grown by the vapor diffusion method at 20 °C using a hanging-drop setup. PBP1b* was crystallized by mixing 1 μL of protein sample (5.0−7.0 mg mL^{-1}, 20 mM HEPES pH 7.0, 100 mM NaCl, 1.0 mM EDTA) and 1 μL of reservoir solution (0.7−0.8 ammonium sulfate, 50 mM HEPES pH 7.2). Crystal soaks were performed by slowly adding saturated ligand solutions prepared in DMSO (to a final concentration of 5%) directly to the crystallization drop. Crystals were mounted in cryoloops and flash-frozen under liquid nitrogen.

Data Collection and Structure Solution. All data (four complexes and an apo PBP1b* data set) were collected under a cold nitrogen stream at 100 K at the European Synchrotron Radiation Facility (Grenoble) on beamline MASSIF-1 (ID30A-1) and were indexed and scaled using XDS.[43] ADVX (https://www.scripps.edu/tainer/arvai/adxv.html) and XDSGUI (https://strucbio.biologie.uni-konstanz.de/xdswiki/index.php/XDSGUI) were used to perform data quality, and STARANISO (https://staraniso.globalphasing.org/cgi-bin/staraniso.cgi) was used for resolution cutoff verification. The reduced X-ray diffraction data were imported into the CCP4-7.1 program suite.[44] Structures were solved by molecular replacement using PHASER[45] and employing the coordinates of PBP1b (PDB:

https://doi.org/10.1021/acschembio.2c00503
ACS Chem. Biol. XXXX, XXX, XXX−XXX

2BG4[16]) lacking residues 460, 516−518, and 650−661 as a search model. The models were then rebuilt *de novo* to remove bias, as implemented in ARP/wARP 7.1.1.[46] The structures were completed by cycles of manual model building with COOT 0.8.9.2.[47] Water molecules were added to the residual electron density map as implemented in ARP/wARP and COOT. Crystallographic macromolecular refinement was performed with REFMAC 5.5.[48] Several cycles of manual model building and refinement were performed until R_{work} and R_{free} converged.[49,50] At this point, the TLS definition was determined and validated using the TLSMD and PARVATI servers.[51,52] The stereochemical quality of the refined models was verified with MOLPROBITY, as implemented in COOT, and PROCHECK.[53,54] Due to the high concentration of NaCl employed in crystallization as well as optimal H-bonding parameters, a Cl^- ion was modeled into a sphere of high electron density within the active site.[55] The secondary structure assignment was performed by DSSP and STRIDE.[56,57] Data collection and refinement statistics are included in Supporting Information Table 1. All solved structures displayed between 99.5 and 100% of the non-glycine residues in the most favored and allowed regions of the Ramachandran plot. Figures containing protein structures were generated with PYMOL (http://www.pymol.org). Final refined model coordinates and structure factors were deposited in the Protein Data Bank (PDB, http://www.rcsb.org), PDB codes: 7ZUH, 7ZUI, 7ZUJ, 7ZUK, 7ZUL.

■ ASSOCIATED CONTENT

Supporting Information

The Supporting Information is available free of charge at https://pubs.acs.org/doi/10.1021/acschembio.2c00503.

Synthesis schemes, gel-band analyses, molecular dynamics RMSF/RMSD plots, crystallographic data collection and refinement statistics, and procedures for cell culture, labeling, cell lysis, and gel electrophoresis (PDF)

■ AUTHOR INFORMATION

Corresponding Authors

Erin E. Carlson − *Department of Medicinal Chemistry, University of Minnesota, Minneapolis, Minnesota 55454, United States; Department of Chemistry, University of Minnesota, Minneapolis, Minnesota 55455, United States; Department of Biochemistry, Molecular Biology, and Biophysics and Department of Pharmacology, University of Minnesota, Minneapolis, Minnesota 55454, United States;* orcid.org/0000-0001-8287-8893; Email: carlsone@umn.edu

Elizabeth A. Ambrose − *Department of Medicinal Chemistry, University of Minnesota, Minneapolis, Minnesota 55454, United States; Minnesota Supercomputing Institute for Advanced Computational Research, University of Minnesota, Minneapolis, Minnesota 55455, United States;* orcid.org/0000-0003-4275-3513; Email: ambrose@umn.edu

Authors

Parker L. Flanders − *Department of Medicinal Chemistry, University of Minnesota, Minneapolis, Minnesota 55454, United States*

Carlos Contreras-Martel − *Université Grenoble Alpes, CNRS, CEA, Institut de Biologie Structurale (IBS), F-38044 Grenoble, France*

Nathaniel W. Brown − *Department of Chemistry, University of Minnesota, Minneapolis, Minnesota 55455, United States*

Joshua D. Shirley − *Department of Medicinal Chemistry, University of Minnesota, Minneapolis, Minnesota 55454, United States*

Alexandre Martins − *Université Grenoble Alpes, CNRS, CEA, Institut de Biologie Structurale (IBS), F-38044 Grenoble, France*

Kelsie N. Nauta − *Department of Chemistry, University of Minnesota, Minneapolis, Minnesota 55455, United States*

Andréa Dessen − *Université Grenoble Alpes, CNRS, CEA, Institut de Biologie Structurale (IBS), F-38044 Grenoble, France; Brazilian Biosciences National Laboratory (LNBio), CNPEM, Campinas 13084-971 São Paulo, Brazil;* orcid.org/0000-0001-6487-4020

Complete contact information is available at: https://pubs.acs.org/10.1021/acschembio.2c00503

Author Contributions

[%]N.W.B., J.D.S.: These authors contributed equally.

Author Contributions

E.A.A. contributed to the design and completion of this project, especially related to molecular modeling and structural analysis, and assisted with manuscript editing. N.W.B. initiated this project, including design and analysis of bioorthogonal lactone-based probes, and assisted with manuscript editing. E.E.C. contributed to the design and completion of this project, especially related to probe design and use, and assisted with manuscript editing. C.C-M. performed crystal soaking experiments, data collection, solution, and refinement of all crystal structures and prepared all crystallography-related figures. A.D. contributed to the design and completion of this project, especially related to protein crystallography, and assisted with manuscript editing. P.L.F. performed molecular modeling, MD simulations, and analysis and prepared the introductory figure as well as all simulation-related figures. A.M. performed expression, purification, and crystallization of PBP1b*. K.N. obtained gel data for probes **5Az** and **6Az**. J.D.S. initiated this project, including the design and analysis of bioorthogonal lactone-based probes, and assisted with manuscript editing.

Notes

The authors declare no competing financial interest.

■ ACKNOWLEDGMENTS

This work used the platforms of the Grenoble Instruct-ERIC center (ISBG; UAR 3518 CNRS-CEA-UGA-EMBL) within the Grenoble Partnership for Structural Biology (PSB), supported by FRISBI (ANR-10-INBS-0005-02) and GRAL, financed within the University Grenoble Alpes graduate school (Ecoles Universitaires de Recherche) CBH-EUR-GS (ANR-17-EURE-0003). This work was also supported by the National Institutes of Health (R01 GM128439 A1, E.E.C. and E.A.A.), the University of Minnesota Department of Chemistry, the University of Minnesota Department of Medicinal Chemistry, and the Minnesota Supercomputing Institute for Advanced Computational Research (MSI). P.L.F. was partly supported by NIH/NIGMS Chemistry-Biology Interface Training Grant 5T32-GM008700. N.W.B. was supported by NIH Institutional Research and Academic Career Development Award K12 GM119955. J.D.S. was supported by the National Institutes of Health's National Center for Advancing Translational Sciences, grants TL1R002493 and UL1TR002494. The content is solely the responsibility of the authors and does not necessarily represent the official views of the National Institutes of Health's National Center for Advancing Translation Sciences. The authors thank

the M. Winkler Lab at Indiana University for providing *S. pneumoniae* strains. Graphical figures were created with GraphPad Prism and BioRender.

REFERENCES

(1) Vollmer, W.; Blanot, D.; De Pedro, M. A. Peptidoglycan structure and architecture. *FEMS Microbiol. Rev.* **2008**, *32*, 149−167.
(2) Alexander, J. A. N.; et al. Structural and kinetic analyses of penicillin-binding protein 4 (PBP4)-mediated antibiotic resistance in Staphylococcus aureus. *J. Biol. Chem.* **2018**, *293*, 19854−19865.
(3) Contreras-Martel, C.; Dahout-Gonzalez, C.; Martins, A. D. S.; Kotnik, M.; Dessen, A. PBP active site flexibility as the key mechanism for beta-lactam resistance in pneumococci. *J. Mol. Biol.* **2009**, *387*, 899−909.
(4) Lim, D.; Strynadka, N. C. J. Structural basis for the β lactam resistance of PBP2a from methicillin-resistant Staphylococcus aureus. *Nat. Struct. Biol.* **2002**, *9*, 870−876.
(5) Moon, T. M.; et al. The structures of penicillin-binding protein 4 (PBP4) and PBP5 from Enterococci provide structural insights into β-lactam resistance. *J. Biol. Chem.* **2018**, *293*, 18574−18585.
(6) Nikolaidis, I.; Favini-Stabile, S.; Dessen, A. Resistance to antibiotics targeted to the bacterial cell wall. *Protein Sci.* **2014**, *23*, 243.
(7) Miyachiro, M. M.; Contreras-Martel, C.; Dessen, A. Penicillin-Binding Proteins (PBPs) and Bacterial Cell Wall Elongation Complexes. *Subcell. Biochem.* **2019**, *93*, 273−289.
(8) Egan, A. J. F.; Errington, J.; Vollmer, W. Regulation of peptidoglycan synthesis and remodelling. *Nat. Rev. Microbiol. 2020* **2020**, *18*, 446−460.
(9) Contreras-Martel, C.; et al. Molecular architecture of the PBP2−MreC core bacterial cell wall synthesis complex. *Nat. Commun.* **2017**, *8* (1), 776.
(10) Den Blaauwen, T.; De Pedro, M. A.; Nguyen-Distèche, M.; Ayala, J. A. Morphogenesis of rod-shaped sacculi. *FEMS Microbiol. Rev.* **2008**, *32*, 321−344.
(11) Mattei, P.-J.; Neves, D.; Dessen, A. Bridging cell wall biosynthesis and bacterial morphogenesis. *Curr. Opin. Struct. Biol.* **2010**, *20*, 749−755.
(12) Meeske, A. J.; et al. SEDS proteins are a widespread family of bacterial cell wall polymerases. *Nature* **2016**, *537*, 634−638.
(13) Rohs, P. D. A.; et al. A central role for PBP2 in the activation of peptidoglycan polymerization by the bacterial cell elongation machinery. *PLOS Genet.* **2018**, *14*, No. e1007726.
(14) Morlot, C.; et al. Crystal structure of a peptidoglycan synthesis regulatory factor (PBP3) from Streptococcus pneumoniae. *J. Biol. Chem.* **2005**, *280*, 15984−15991.
(15) Wahl, B.; et al. Burden of Streptococcus pneumoniae and Haemophilus influenzae type b disease in children in the era of conjugate vaccines: global, regional, and national estimates for 2000−15. *Lancet Glob. Heal.* **2018**, *6*, e744−e757.
(16) Macheboeuf, P.; et al. Active site restructuring regulates ligand recognition in class A penicillin-binding proteins. *Proc. Natl. Acad. Sci. U. S. A.* **2005**, *102*, 577−582.
(17) Andrejko, K.; Ratnasiri, B.; Lewnard, J. A. Association of Pneumococcal Serotype With Susceptibility to Antimicrobial Drugs: A Systematic Review and Meta-analysis. *Clin. Infect. Dis.* **2022**, *75*, 131−140.
(18) Vollmer, W.; Massidda, O.; Tomasz, A. The Cell Wall of Streptococcus pneumoniae. *Microbiol. Spectr.* **2019**, DOI: 10.1128/microbiolspec.GPP3-0018-2018.
(19) Bellini, D.; Koekemoer, L.; Newman, H.; Dowson, C. G. Novel and Improved Crystal Structures of H. influenzae, E. coli and P. aeruginosa Penicillin-Binding Protein 3 (PBP3) and N. gonorrhoeae PBP2: Toward a Better Understanding of β-Lactam Target-Mediated Resistance. *J. Mol. Biol.* **2019**, *431*, 3501−3519.
(20) Levy, N.; et al. Structural Basis for E. coli Penicillin Binding Protein (PBP) 2 Inhibition, a Platform for Drug Design. *J. Med. Chem.* **2019**, *62*, 4742−4754.
(21) Macheboeuf, P.; et al. Structural and mechanistic basis of penicillin-binding protein inhibition by lactivicins. *Nat. Chem. Biol.* **2007**, *3*, 565−569.
(22) Rajavel, M.; et al. Structural Characterization of Diazabicyclooctane β-Lactam 'Enhancers' in Complex with Penicillin-Binding Proteins PBP2 and PBP3 of Pseudomonas aeruginosa. *MBio* **2021**, *12*, 1−18.
(23) Singh, A.; Tomberg, J.; Nicholas, R. A.; Davies, C. Recognition of the β-lactam carboxylate triggers acylation of Neisseria gonorrhoeae penicillin-binding protein 2. *J. Biol. Chem.* **2019**, *294*, 14020−14032.
(24) Macheboeuf, P.; Contreras-Martel, C.; Job, V.; Dideberg, O.; Dessen, A. Penicillin binding proteins: key players in bacterial cell cycle and drug resistance processes. *FEMS Microbiol. Rev.* **2006**, *30*, 673−691.
(25) Contreras-Martel, C.; et al. Structure-guided design of cell wall biosynthesis inhibitors that overcome β-lactam resistance in staphylococcus aureus (MRSA). *ACS Chem. Biol.* **2011**, *6*, 943−951.
(26) Kocaoglu, O.; et al. Selective penicillin-binding protein imaging probes reveal substructure in bacterial cell division. *ACS Chem. Biol.* **2012**, *7*, 1746−1753.
(27) Kocaoglu, O.; Carlson, E. E. Profiling of β-lactam selectivity for penicillin-binding proteins in Escherichia coli strain DC2. *Antimicrob. Agents Chemother.* **2015**, *59*, 2785−2790.
(28) Kocaoglu, O.; Tsui, H. C. T.; Winkler, M. E.; Carlson, E. E. Profiling of β-lactam selectivity for penicillin-binding proteins in Streptococcus pneumoniae D39. *Antimicrob. Agents Chemother.* **2015**, *59*, 3548−3555.
(29) Böttcher, T.; Sieber, S. A. Beta-lactones as privileged structures for the active-site labeling of versatile bacterial enzyme classes. *Angew. Chem., Int. Ed. Engl.* **2008**, *47*, 4600−4603.
(30) Böttcher, T.; Sieber, S. A. β-Lactams and β-lactones as activity-based probes in chemical biology. *Medchemcomm* **2012**, *3*, 408−417.
(31) Sharifzadeh, S.; et al. Novel Electrophilic Scaffold for Imaging of Essential Penicillin-Binding Proteins in Streptococcus pneumoniae. *ACS Chem. Biol.* **2017**, *12*, 2849−2857.
(32) Konaklieva, M. I. Molecular Targets of β-Lactam-Based Antimicrobials: Beyond the Usual Suspects. *Antibiot. (Basel, Switzerland)* **2014**, *3*, 128−142.
(33) Brown, N. W.; Shirley, J. D.; Marshall, A. P.; Carlson, E. E. Comparison of Bioorthogonal β-Lactone Activity-Based Probes for Selective Labeling of Penicillin-Binding Proteins. *ChemBioChem.* **2021**, *22*, 193−202.
(34) Sharan, D.; Carlson, E. E. Expanded profiling of β-lactam selectivity for penicillin-binding proteins in Streptococcus pneumoniae D39. *Biol. Chem.* **2022**, *403*, 433−443.
(35) Laskowski, R. A.; Swindells, M. B. LigPlot+: multiple ligand-protein interaction diagrams for drug discovery. *J. Chem. Inf. Model.* **2011**, *51*, 2778−2786.
(36) Macheboeuf, P.; et al. Trapping of an acyl-enzyme intermediate in a penicillin-binding protein (PBP)-catalyzed reaction. *J. Mol. Biol.* **2008**, *376*, 405−413.
(37) Hess, B. Convergence of sampling in protein simulations. *Phys. Rev. E* **2002**, *65*, No. 031910.
(38) Sauvage, E.; Kerff, F.; Terrak, M.; Ayala, J. A.; Charlier, P. The penicillin-binding proteins: structure and role in peptidoglycan biosynthesis. *FEMS Microbiol. Rev.* **2008**, *32*, 234−258.
(39) Kumarasiri, M.; Zhang, W.; Shi, Q.; Fisher, J. F.; Mobashery, S. Protonation States of Active-Site Lysines of Penicillin-Binding Protein 6 from Escherichia coli and the Mechanistic Implications. *Proteins* **2014**, *82*, 1348.
(40) Madhavi Sastry, G.; Adzhigirey, M.; Day, T.; Annabhimoju, R.; Sherman, W. Protein and ligand preparation: Parameters, protocols, and influence on virtual screening enrichments. *J. Comput. Aided. Mol. Des.* **2013**, *27*, 221−234.
(41) Bowers, K. J.; et al. Scalable algorithms for molecular dynamics simulations on commodity clusters. *Proc. 2006 ACM/IEEE Conf. Supercomput. SC'06* **2006**, DOI: 10.1145/1188455.1188544.

(42) Michaud-Agrawal, N.; Denning, E. J.; Woolf, T. B.; Beckstein, O. MDAnalysis: A Toolkit for the Analysis of Molecular Dynamics Simulations. *J. Comput. Chem.* **2011**, *32*, 2319.
(43) Kabsch, W. Automatic processing of rotation diffraction data from crystals of initially unknown symmetry land cell constants. *J. Appl. Crystallogr.* **1993**, *26*, 795−800.
(44) Winn, M. D.; et al. Overview of the CCP4 suite and current developments. *Acta Crystallogr. D. Biol. Crystallogr.* **2011**, *67*, 235−242.
(45) Storoni, L. C.; McCoy, A. J.; Read, R. J. Likelihood-enhanced fast rotation functions. *Acta Crystallogr. D. Biol. Crystallogr.* **2004**, *60*, 432−438.
(46) Cohen, S. X.; et al. ARP/wARP and molecular replacement: the next generation. *Acta Crystallogr. Sect. D Biol. Crystallogr.* **2008**, *64*, 49.
(47) Emsley, P.; Cowtan, K. Coot: model-building tools for molecular graphics. *Acta Crystallogr. D. Biol. Crystallogr.* **2004**, *60*, 2126−2132.
(48) Murshudov, G. N.; et al. REFMAC5 for the refinement of macromolecular crystal structures. *Acta Crystallogr. D. Biol. Crystallogr.* **2011**, *67*, 355−367.
(49) Brünger, A. T. Free R value: a novel statistical quantity for assessing the accuracy of crystal structures. *Nature* **1992**, *355*, 472−475.
(50) Holton, J. M.; Classen, S.; Frankel, K. A.; Tainer, J. A. The R-factor gap in macromolecular crystallography: an untapped potential for insights on accurate structures. *FEBS J.* **2014**, *281*, 4046−4060.
(51) Painter, J.; Merritt, E. A. Optimal description of a protein structure in terms of multiple groups undergoing TLS motion. *Acta Crystallogr. D. Biol. Crystallogr.* **2006**, *62*, 439−450.
(52) Zucker, F.; Champ, P. C.; Merritt, E. A. Validation of crystallographic models containing TLS or other descriptions of anisotropy. *Acta Crystallogr., Sect. D: Biol. Crystallogr.* **2010**, *66*, 889−900.
(53) Chen, V. B.; et al. MolProbity: all-atom structure validation for macromolecular crystallography. *Acta Crystallogr. D. Biol. Crystallogr.* **2010**, *66*, 12−21.
(54) Laskowski, R. A.; MacArthur, M. W.; Moss, D. S.; Thornton, J. M.; IUCr. PROCHECK: a program to check the stereochemical quality of protein structures. *J. Appl. Crystallogr.* **1993**, *26*, 283−291.
(55) Echols, N.; et al. Automated identification of elemental ions in macromolecular crystal structures. *Acta Crystallogr. Sect. D Biol. Crystallogr.* **2014**, *70*, 1104−1114.
(56) Kabsch, W.; Sander, C. Dictionary of protein secondary structure: pattern recognition of hydrogen-bonded and geometrical features. *Biopolymers* **1983**, *22*, 2577−2637.
(57) Heinig, M.; Frishman, D. STRIDE: a web server for secondary structure assignment from known atomic coordinates of proteins. *Nucleic Acids Res.* **2004**, *32*, W500.

https://doi.org/10.1021/acschembio.2c00503
ACS Chem. Biol. XXXX, XXX, XXX−XXX